Magnetic Nanoclusters Synthesized by a Novel Method of Aggregation in Ultra High Vacuum; Applications in Nanoelectronics and Nanomedicine

O. Crisan, A.D. Crisan

National Institute for Materials Physics, P.O. Box MG-7
077125 Bucharest-Magurele, Romania
E-mail: ocrisan@yahoo.com

Abstract. A novel method for producing metal clusters as building blocks for nanoscale devices is reported and its advantages for nanoelectronics and biomedical applications are highlighted. The method, which is a derivative from the wider range of techniques called the gas / cluster aggregation methods, is suitable to synthesise nano-clusters of various nature (metallic, oxides, hybrid core-shell architectures) in a wide range of sizes, from submonolayers (few hundreds of atoms clusters) to continuous thin films. More important, these clusters may be subsequently modified and functionalized *in-situ* by adding atoms/molecules of different nature, on the surface of readily formed clusters. The cluster size is extremely well controlled by the vapor pressure of the picked-up species. Moreover, the method is versatile, since it allows multiple pick-up processes within the same rare gas cluster to produce, for example, core-shell nanoparticles with metal core and non-metallic shell or vice-versa, nano-onions, with different species successively attached to the surface of the initial picked-up cluster, and so on. Initial formation of Fe gas-stabilised clusters and core-shell nanoparticles with Fe core and Fe oxide shell, as well as their structure and morphology, are presented and discussed. The core-shell nanoparticles show incipient self-organization into hexagonal cluster superlattice. Structural, magnetic and Mössbauer spectroscopy investigations have been performed on the Fe cluster samples. The magnetic properties of supported Fe clusters show marked differences compared to the bulk. A small hysteresis is observed in the parallel applied field while in the perpendicular case, lack of saturation at the highest applied field is noticed. Such behaviour has been also observed in FeRh [1] and AgCo [2] bimetallic nanoparticles. This behaviour marks the occurrence of a strong planar magnetic anisotropy in the sample and may also be a consequence of increased surface spin disorder and finite size effects, which are typical for nanoparticles in the reported size range.

Keywords: Nanoclusters, Core-shell nanoparticles, Surface-functionalization, Gas/cluster aggregation method

1. Introduction

The production and functionalization of nanometric sized materials with outstanding magnetic, optic and electronic properties has attracted a large interest

in the last years. The more and more developed methods of synthesis allow now complex architectures of nano-objects to be created. Moreover, these systems may be functionalized with molecules, free radicals, and so on, for a wide range of applications. Magnetic clusters may be produced with a strict size and shape control and may serve as templates for surface attachment of molecules for specific biomedical applications. For example, such metallic clusters may be surface-functionalized for the use in biomedical applications as DNA markers, as contrast-enhancement agents in magnetic resonance imaging or as drug delivery media [3]. The magnetic properties of such clusters are highly dependent on the size of the clusters. It has been shown [4] that such clusters are ferromagnetic for the smallest sizes: clusters with less than 30 atoms the magnetic moments are close to the atomic value, while if size is increased up to 700 atoms, the magnetic moments approach the bulk limit. Very large orbital moments were obtained for Co clusters on Pt [5], or Fe clusters on Cu [6] and Mo [7]. Also, bimetallic clusters of Co-Mn were reported to have enhanced magnetic moments compared with the bulk [8] and Co clusters embedded in Mn have been shown to exhibit exchange bias effect [9]. It is of interest to note that the magnetic properties of such systems are different if studied as free clusters or supported onto various surfaces. Different magnetic configurations resulting from the interplay of various interparticle interactions are possible, depending on a wide range of factors, from the nature, size and shape of clusters, to the nature of supporting substrate, density and volume fraction of the magnetic nano-objects and so on. It has been shown that in isolated Fe nanoparticles with strong surface anisotropy, the surface spin configuration evolves towards a throttled spin state that imposes altered magnetic properties on the whole system [10]. Also, in the case of bimetallic AgCo core-shell nanoparticles, strong non-saturation effects on the magnetization, due to the particular coronal shape of the magnetic element (Co) were observed [11]. Fe nanoclusters produced from the gas phase [12] exhibit an enhancement of both orbital and spin moments as compared to the bulk. Subsequent coating of Fe clusters with Co creates a further increase of the spin moment without significantly changing the orbital moment [12]. It has been shown [13] that depending on the volume fractions of Fe clusters, the interplay of dipolar and exchange coupling interactions create a wide range of possible magnetic configurations. These configurations range from superparamagnetism (SPM) with or without interactions, for low cluster volume fraction, up to collective blocking and correlated spin glass states, for high cluster volume fractions [13].

The cluster aggregation methods, is an extremely versatile path for producing isolated, small clusters of aggregated atoms, molecules, free radicals and so on. The principle of this method is based on producing a beam of cold rare gas in supersonic expansion. The beam is produced in the source chamber and picks-up single atoms and molecules from an evaporator in a UHV multi-chamber. The technique, developed for fundamental studies of free clusters of atoms and

molecules, that employs Ag clusters [14, 15] or liquid He droplets [16, 17], has been proven to be also effective in producing magnetic metal clusters [18]. The paper reports on the gas-stabilized free cluster aggregation method, the production of free and supported Fe clusters on mica, their structural and morphological properties as well as their correlation with the magnetic behavior of the samples.

2. Experimental

Previous studies on metal clusters have shown that the properties of the clusters are different if studied in molecular beams, or on surfaces or embedded in solid matrices. The method we present hereafter has the advantage of a very rapid pick-up process of the metal vapor by the cold rare gas supersonic beam, followed by a quick (1 ms) condensation inside the beam. For clusters deposited on surfaces and in matrices, the temperature is well known and can be easily varied; however, the substrate or matrix perturbs the clusters. Since a large fraction of the atoms are in surface states, this perturbation can dominate the desired properties.

The synthesis method of cluster aggregation implies the use of a beam of rare gas molecules (Ar), formed within a source chamber. The beam passes through a liquid nitrogen cooled nozzle, which ensures the supersonic flow of the cold rare gas in a region of low-pressure metal vapor (pick-up chamber), created by a resistive heated metal evaporator (crucible). Metal vapors are collected or picked up by the large rare gas molecules in the pick-up zone, are condensed within 1 ms, and cold metal clusters are thus formed within the gas beam. The pick-up process is governed by a Lennard-Jones interaction potential that depends on the nature of the metal vapor to be picked up by the cold rare gas cluster. This beam passes through the plates of a time-of-flight (TOF) mass spectrometer where it is investigated, and / or collected onto suitable placed substrates or grids, in order to determine *ex-situ* their structural features and other properties. The cluster size is extremely well controlled by the vapor pressure of the picked-up species, which in turn is controlled by the temperatures of the heated crucible. The method is versatile, since, by using several aligned evaporators, it allows multiple pick-up processes within the same rare gas cluster beam to produce, for example, core-shell nanoparticles or multiple shells to form nano-onions. Successive layer formation on the initial (metal) core is controlled by partial pressures of the evaporated constituents.

Schematics of the preparation facility

Fig. 1 represents the schematics of the UHV multi-chamber facility used for the production of the free Fe clusters. The first chamber of the UHV facility is the source chamber where the gas beam is formed. This chamber is cooled with liquid nitrogen, through an external shielding. In the middle, the Ar gas is purged towards

the nozzle situated at the other extremity of the chamber. The gas beam enters the pick-up chamber through the skimmer and hits the metal ions that are evaporated by the crucible. The metal vapors are picked up by the rare gas molecules from the incipient beam and are condensed. The gas beam containing the cold metal clusters is investigated in the TOF chamber.

In the specific case presented here, the sample holder, where the TEM grids and substrate for depositing the clusters, was mounted instead of the second evaporator, right in front of the metal crucible, in order to minimize the pathway of the beam and maximize the area exposed to the metal beam. The cluster beam was first investigated in the TOF spectrometer (the sample holder is firstly kept below the incipient cluster beam so as to allow the beam to reach the TOF).

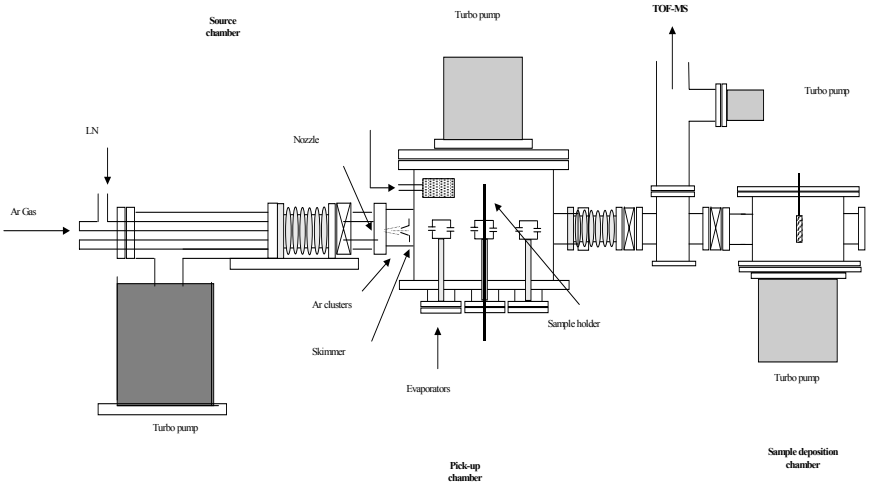

Fig. 1. Schematics of the cluster aggregation UHV multi-chamber facility

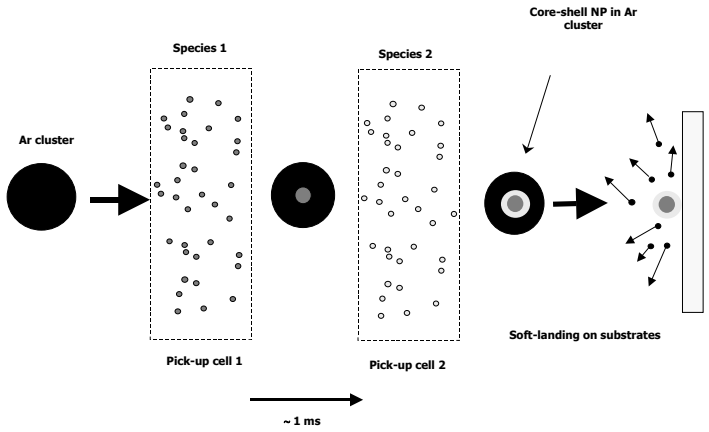

Fig. 2. Schematics of the multiple pick-up process that leads to the production of core-shell NP's.

Inside the main chamber there are several aligned evaporators. As mentioned above, this allows multiple pick-up processes, within the same rare gas beam, to produce core-shell nanoparticles. The schematics of the multiple pick-up processes that take place in the cold rare gas beam are represented in Figure 2. The supersonic beam of Ar molecules penetrates inside the first pick-up zone and loses its kinetic energy by multiple collisions with the metal vapors. These vapors are almost instantly condensed and are retained inside the Ar molecules. The size of the metal clusters is strictly controlled by the partial pressure inside the pick-up zone. Then the beam hits the second pick-up zone and the metal (or other species) vapors from the second evaporator are at their turn embedded into the rare gas molecules, either by forming core-shell nanoparticles or, depending on the degree of miscibility, bimetallic nanoparticles, or, if second species is a molecule or a ligand, a suface-functionalized nanoparticle.

Synthesis conditions and experimental characterization techniques:

The Fe clusters were synthesised as mentioned above, following the fast pick-up / condensation process inside the rare gas supersonic beam. In order to investigate thoroughly their structure and morphology, the beam was directed onto TEM grids where clusters were deposited and thermalized. The subsequent adhesion of the Fe clusters on the grid was eased by an inert gas-flow stabilization process. The synthesis method requires formation of a rare gas beam produced by expansion in a supersonic jet that passes through a conical nozzle into the ultra-high-vacuumed pick-up chamber. The parameters of the cluster beam are essentially related to the shape of the nozzle used. If the nozzle temperature and gas pressure are accurately determined, scaling laws [19,20] allow to precisely determine the size of the rare gas clusters. In our case, the conical nozzle has a throttle diameter of 300 microns and a conical aperture of 15° half-angle. The nozzle temperature was kept at 90K, by the liquid nitrogen flowing in the shielding layer of the cluster source. The input Ar gas pressure was 10^{-3} mbar. The substrates used in the first experiment were TEM copper grids (300 mesh Cu) coated by carbon film. The metal evaporator was carefully out-gassed at high temperature (but well below the melting point) for 12 h. The initial pressure inside the main pick-up chamber was between 10^{-7} and -10^{-8} mbar (depending on the evaporator temperature). Before deposition, the crucible temperature was increased and, in several experiments, varied between 1400K and 1500K so as to ensure a low metal vapor pressure between 10^{-5} and 10^{-4} mbar. The as-formed rare gas beam formed inside the source chamber is sputtered through the nozzle into the pick-up chamber where it undergoes several pick-up processes and is projected onto the TEM grids. Embedding metal atoms into the rare gas beam occur after multiple collisions with the metal vapors. At each collision with the metal atoms, part of the gas atoms from the beam evaporates and upon reaching the target (substrate) the metal cluster

is already formed, as the pick-up processes are much faster than the travel time until the beam reaches the substrate. The pick-up process is governed by the binding energy of the cluster as well as by the Lennard-Jones interaction potential between the gas atoms and picked-up species. Precise *xyz* alignment of the nozzle and implicitly of the direction of the cluster beam was performed, and the nozzle-crucible distance was optimized by measuring the intensities in TOF spectra given by the gas beam, prior to the deposition process. The exposure time for the TEM grids was 5 minutes and the Fe clusters formation of was observed, stabilized on the grids by the subsequent long-time low-pressure rare gas flow. The experimental techniques that we used for structural characterization of the as-obtained samples were:

- Time-of-Flight (TOF) mass spectrometer: as an in-situ rare gas and metal clusters analyser;
- Transmission electron microscopy (TEM): - JEOL 2100 microscope, 2kV acceleration potential, in bright field and high-resolution modes;
- Electron diffraction patterns (EDP): Fourier transforms (reciprocal space map) of TEM images, to identify the crystal symmetry;
- Energy dispersion spectroscopy (EDS): to obtain chemical quantitative analysis of samples;
- Atomic force microscopy: to investigate the topography and morphology of cluster arrangements

3. Results and Discussion

Occurrence of Fe clusters inside the rare gas beam. TOF mass spectrometry

Fig. 3 depicts the TOF mass spectra obtained when only the supersonic Ar gas beam (left) passes through the TOF plates, compared to the one where the metal clusters are condensed and embedded within the original supersonic gas beam. The TOF spectra show the formation of Ar clusters in the beam that passes through the cooled nozzle. Nevertheless, the intensities of the harmonics depicting the formation of gas clusters up to the 14th order are not so high, compared with the gas pressure input into the main chamber.

The conclusion is that the supersonic beam is mostly formed by Ar molecules, with a small fraction of Ar clusters, therefore the pick-up process that allows production of metal clusters is in fact a mixture of gas aggregation and cluster aggregation principles. The right graph depicts the TOF spectrum collected for the gas + metal clusters when the metal evaporator is set at 900K (or 10^{-5} mbar metal vapor pressure). When the gas beam contains also the cold Fe clusters, these Fe clusters are harder to identify in the TOF spectra, mainly due to the high noise level arising from multiple scattering processes inside the TOF, as the partial vapor

pressure is quite high for the TOF measurements. Nevertheless, the peak corresponding to the Fe atomic mass (near 56 atomic mass units) can be seen in the right TOF spectrum. The TOF measurements confirmed that indeed the desired metal clusters are formed inside the rare gas molecular beam.

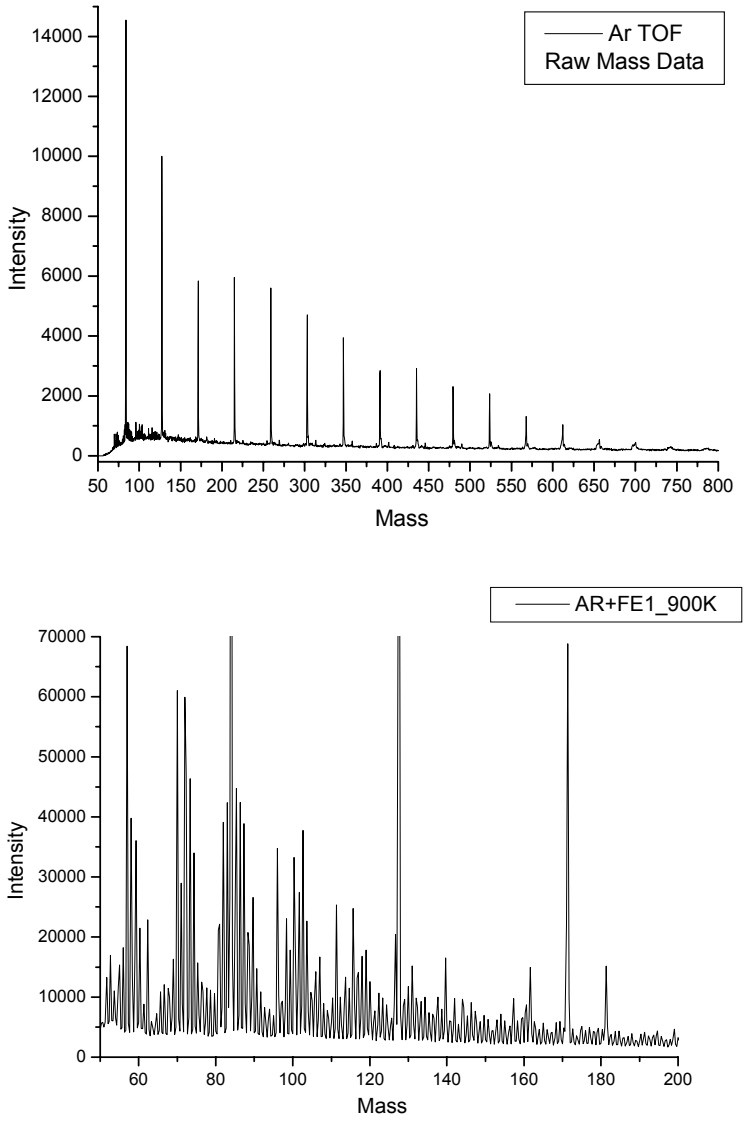

Fig. 3. Time-of-flight mass spectra of the Ar molecular gas beam (top) and the molecular gas beam after picking up the Fe clusters (bottom) evaporated at 900K (10^{-5} mbar).

Structure of Fe clusters on TEM Cu grids

The influence of the metal vapor pressure onto the structure and morphology of the Fe clusters deposited in the above-described UHV facility onto TEM grids, has been largely described elsewhere [22]. Three different deposition experiments with the same exposure time for the grid, but with different partial metal vapor pressures have been performed. The pressure was established by controlling the evaporator temperature. A well-known charted proportional relationship exists between the crucible temperature and the resulted metal vapor pressure [19]. For example, the temperature of 1400K of the metal evaporator corresponds to a metal vapor pressure of 10^{-5} mbar. In the TEM images [25] the as-deposited Fe aggregates are mostly spherical with sizes that increase when the metal vapor pressure increases. No apparent ordering is observed.

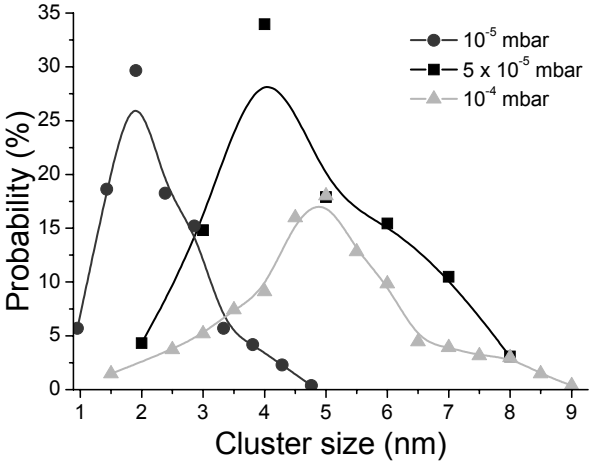

Fig. 4a. The cluster size distributions for samples sputtered at various metal vapor pressures.

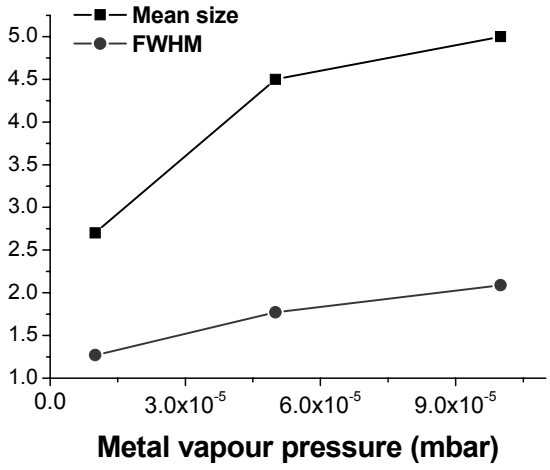

Fig. 4b: The average size obtained by the histographic technique and the width of the log - normal distributions obtained after numerical fittings.

These observations have now been made quantitative. A large number of images have been studied and, using a histographic method, the size distribution for all 3 samples has been derived. The size distributions are plotted in Fig. 4 (a). Average sizes obtained for the Fe clusters were 2.7, 4.5 and 5.1 nm for vapor pressures of 10^{-5}, 5 x 10^{-5} and 10^{-4} mbar respectively. The cluster size distributions approximately obey a log-normal profile law. The average size as well as the full-width-at-half-maximum (FWHM) of the log-normal distributions obtained after numerical fittings is plotted in Figure 4 (b). It can be seen that the size distribution of the obtained Fe clusters are shifted towards larger cluster sizes as the metal vapor pressure increases. Distributions are also larger as the metal vapor pressure increases, as both the average particle size and width of the distribution increases with the vapor pressure. With further increase of the vapor pressure, distributions seem to exhibit tendency towards a bimodal character. It is expected that higher densities and volume fractions (higher exposure times) will lead to cluster aggregation and change of crystal symmetry.

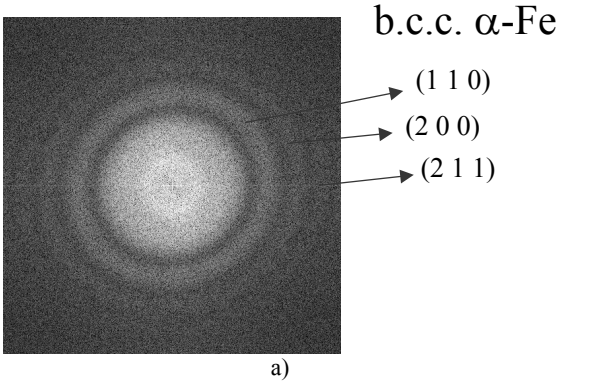

a)

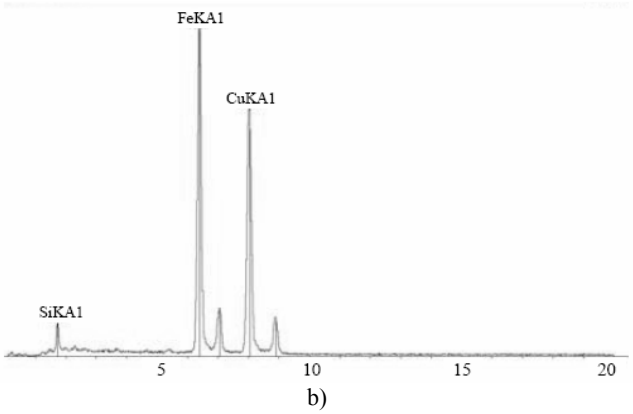

b)

Fig. 5a. Electron diffraction pattern of the Fe clusters showing 3 Bragg reflections of the b.c.c. α-Fe phase symmetry. b. Energy dispersion spectrum of Fe clusters on Cu grid, obtained under a metal vapor pressure of 10^{-4} mbar inside the pick-up chamber.

It is also worthwhile mentioning that in the electron diffraction (EDP) patterns of all samples, recorded during TEM imaging and presented in the Fig. 5a, we have unambiguously identified the diffraction rings corresponding to (1 1 0), (2 0 0) and (2 1 1) Bragg reflections of the body-centred-cubic α-Fe. It seems that the deposited Fe clusters have a cubic symmetry whatever the metal vapor pressure during the deposition, at least up to 10^{-4} mbar. As mentioned above, it is expected that higher metal vapor pressures and / or exposure times (with impact on the effective volume fraction of the film) would lead to changes in the structural symmetry of the Fe clusters. Also, during TEM imaging, energy dispersion X-ray spectroscopy (EDX) was undertaken in order to check the chemical elemental composition of the grids. An example of such spectra is plotted in Fig. 5b. It has been observed that only Fe $K\alpha_1$ and Cu $K\alpha_1$ peaks appear in the spectra. At this point, no oxidation was observable through the chemical analysis of the Fe clusters on the TEM grids.

Structure of core-shell Fe / Fe oxide nanoclusters

The Fe/Fe oxide core-shell nanoparticles were also produced in a very simple way, by allowing the Fe containing rare gas molecular supersonic beam to enter a region with controlled partial pressure of oxygen. In the way described earlier, with successive pick-up processes, we expected to see a core-shell structure where the Fe core is surrounded by a Fe oxide layer of uniform size. That was indeed the case, as it is shown in the bright field TEM image of these Fe/Fe oxide clusters. In Figure 5 it is shown a TEM image of the core-shell Fe/Fe oxide nanoparticles, formed by the gas-stabilization method. In this image, and also in the following ones, one can observe the occurrence of multiple-faceted core-shell NP's of a white core and a dark shell, with a somehow regular coronal thickness, as intended. It is clear that in the first step, of metal vapor condensation, inside or on the surface of the rare gas molecule, a spherical metal cluster is formed. Afterwards, the metal oxide surrounding the metal core is grown as a complete covering coronal layer onto the metal core surface, simply by allowing controlled pressure of oxygen to enter the UHV pick-up region. The oxygen pressure was 1.1×10^{-3} mbar. The TEM grid was subjected to the oxygen pressure for about 1 hour, time long enough to grow a continuous oxide layer around the metal core, and then the oxygen flux was switched off. A beginning of an ordering seems to occur as in the highlighted part of the image. Hexagonal "crystals" of Fe clusters self-organized into what looks like an icosahedral-type superlattice. It seems that during the oxidation process, a stable (minimum energy) configuration is achieved, and the core-shell clusters commence to self-organize. This phenomenon has been observed to occur in Ag-Au bimetallic nanoclusters [23] and the array formed, of an icosahedral symmetry, has been named as "cluster of clusters". The phenomenon, explained by the balance between kinetic energy of the incoming clusters hitting the substrate and

the thermal energy gained by the evaporation of the gaseous carrier (the rare gas cluster) allow a commencement of the self-organization process into a quasi-regular array of icosahedral symmetry. Nevertheless, the energy gained via the stabilization process is not enough to allow periodic arrangement onto larger arrays, as it is the case during the stabilization of chemically obtained nanoparticles during the colloidal crystallization from solution [11,24], that allows the observation of large periodic arrays of monodispersed nanoparticles, practically onto the whole area of the substrate. However, the purpose of the experiment, i.e. the production of core-shell nanoparticles with metal core and continuous, uniformly thick shell of metal oxide, has been accomplished.

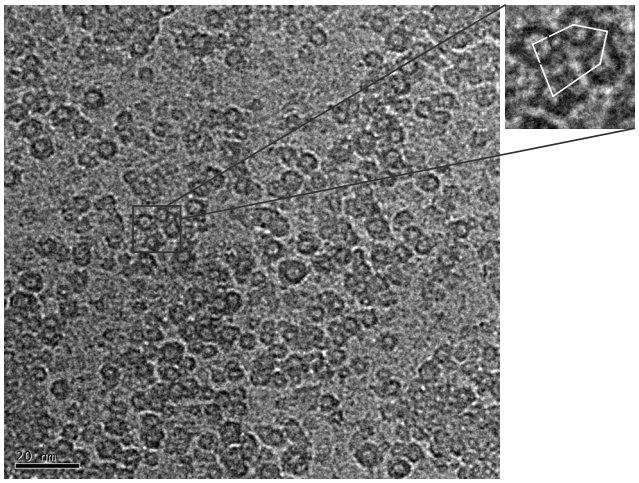

Fig. 6. TEM image of an assembly of Fe / Fe oxide dispersed nanoparticles. Inset: formation of icosahedral- type superlattice, taken from [25].

In order to provide more complete morpho-structural characterization of the core-shell clusters, we have performed atomic force microscopy using an Omicron instrument in high vacuum. The grids were mounted on stainless steel holder and a cantilever with Si tip was used for scanning the grid surface. An AFM image recorded during the experiment together with a cross section line profile is shown in Fig. 7.

The atomic force microscopy image shows columnar-like growth of aggregates of sizes compatible with TEM observations. Their intrinsic features are hidden by the averaging of the atomic potential, developed by the cantilever tip, over the surface. The height of the cluster aggregates observed in the image is about 10 nm, a value comparable with the cluster sizes obtained from TEM, taking into account also the tip-surface interaction that gives slightly higher topographical features. A 4 nm periodicity is observed in the line profile of the Fe clusters (Figure 7b), which again, is comparable to the average cluster size observed in TEM.

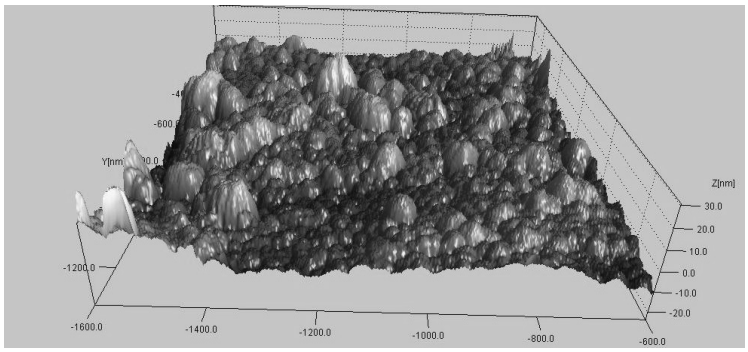

a)

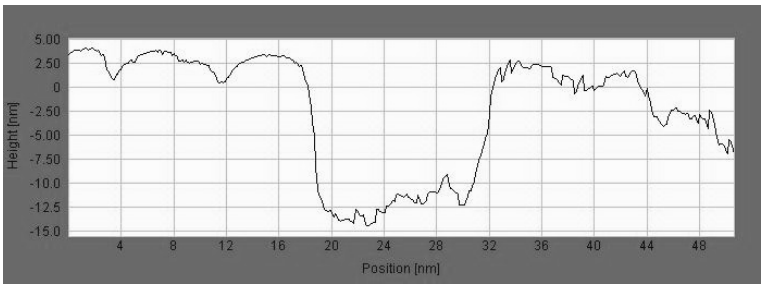

b)

Fig. 7. Atomic force microscopy of core-shell nanoparticles (a) and cross - section line profile of the imaged topography (b).

This first experiment to produce core-shell clusters in our cluster aggregation UHV facility opens wide perspectives into production of several types of core-shell clusters and other nano-architectures including, for example cores with multiple shells. These surface shells may be furthermore surface-functionalized for example, by attaching molecules, ligands, proteins, receptors, for a huge number of biomedical applications, but also for other kind of technological applications such as catalysis or nanosensors. One of the envisaged future applications is formation of high anisotropic – high magnetic moment core surrounded by Au layer coating, and attachment onto this coating of various biological proteins as DNA markers or tumor markers such as aptamers or folic acid [3].

Structure of the Fe clusters supported on mica substrate

In order to further investigate other macroscopic properties, samples of Fe clusters were also deposited onto mica substrate. In this experiment, instead of TEM grids, pure muscovite clean sheets were mounted onto the holder. Metal vapor pressure was fixed at 10^{-4} mbar with a crucible temperature of 1500K. Due to the fact that, for other types of measurements, such as Mossbauer or magnetism,

larger amounts of Fe clusters are necessary in order to observe a noticeable effect, we have chosen to increase the exposure time up to 30 minutes. The structure of the as-obtained Fe clusters on mica was examined *ex-situ* by powder X-ray diffraction using Cu Kα radiation (wavelength: λ=1.54Å). A well-resolved spectrum with sharp Bragg peaks is obtained, as seen in Figure 8. It may be noticed that a very strong contribution to the XRD spectrum arises from the mica substrate. This is an expected effect since the mass of the mica substrate is much lager than the amount of supported Fe clusters.

As depicted in the Figure 8, the Bragg reflections attributed to the $2M_1$ phase structure of mica (muscovite) are indexed. In spite of that, we have been able to identify the contribution from the supported Fe clusters, too. The diffraction peaks arising from the (1 1 0), (2 0 0) and (2 1 1) Bragg reflections of the body-centred-cubic α-Fe structure are also observed and correctly indexed. These results are in agreement with TEM observations of free Fe clusters, synthesised at a much lower exposure time (5 min compared to 30 min). The two measurements may thus be correlated in spite of the exposure time difference since no change in crystal symmetry is observed, compared to the free Fe clusters.

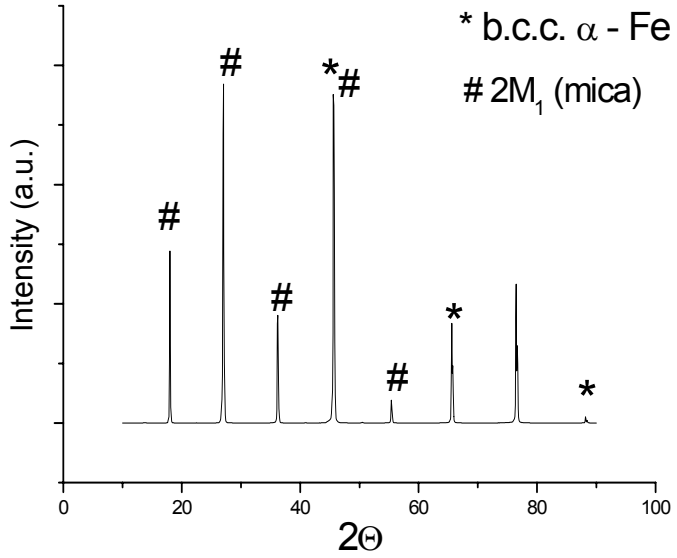

Fig. 8. X-ray diffraction spectrum of the supported Fe clusters on mica.

Mössbauer data on supported Fe clusters on mica

One of the reasons for choosing mica as the substrate for the supported Fe clusters was its transparency to the γ-rays, so that the sample could be investigated by Mössbauer spectroscopy. The Mössbauer spectrum recorded at room temperature in transmission geometry is presented in Fig. 9.

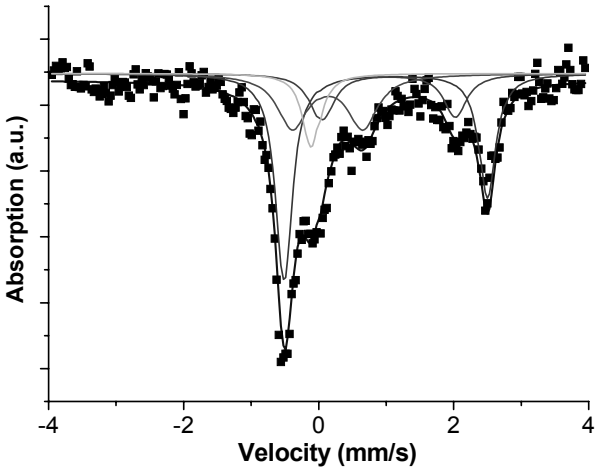

Fig. 9. Mössbauer spectrum of Fe clusters supported on mica.

We first noticed that the supported Fe clusters are not ferromagnetic at room temperature, since there was no magnetic Zeeman splitting of the Mössbauer spectrum. This is an expected effect since the volume fraction is not so large, even at 30 minutes time of exposure to the cluster beam. As the metal vapor pressure was kept at a relatively low value (10^{-4} mbar) the deposition rate was low. Four different contributions were revealed from the fitting of the Mössbauer spectrum. Two doublets with high quadrupole splitting were fitted to the experimental spectrum and attributed to the octahedral Fe^{2+} cis and trans sites of the $2M_1$ structure of mica. Another doublet with lower quadrupole splitting has been attributed to the octahedral Fe^{3+}. This assignation is in agreement with previously reported site population of the Fe-muscovite from Mössbauer data [26]. The singlet in the central part of the spectrum, having an isomer shift value close to 0, is attributed to the superparamagnetic metallic Fe clusters having a b.c.c. structure. The Fe clusters contribution observed in the Mössbauer spectrum has an abundance of 10%. These results are in agreement with TEM observations of free Fe clusters and XRD structural data. From Mössbauer data it seems that the clusters behave as an assembly of non-interacting superparamagnets. All the hyperfine parameters obtained from the Mössbauer spectrum fitting are presented in Table 1.

Table 1. Hyperfine parameters of the Mössbauer spectrum of Fe film on mica.

	Isomer shift (mm/s)	Quadrupole splitting (mm/s)	Relative area (%)
I: $2M_1$ octahedral Fe^{2+} cis	1.12	2.98	46
II: $2M_1$ octahedral Fe^{2+} trans	1.16	1.96	17
III: $2M_1$ octahedral Fe^{3+}	0.26	1.01	27
IV: SPM metallic Fe (b.c.c.)	0.03	0.00	10

Magnetic properties

The room temperature hysteresis loops for supported Fe clusters on mica were measured in a vibrating sample magnetometer at an applied field of up to 0.8 Tesla, both parallel and perpendicular to the substrate plane. As it is well known, bulk Fe in the b.c.c. crystalline symmetry is magnetically soft with virtually no hysteresis, and high saturation magnetization. As it can be seen in the two hysteresis loops, plotted in Figure 10, a quite different behavior from the bulk is obtained.

The hysteresis loop recorded parallel to the substrate plane exhibits interesting magnetic behavior. In the case of the parallel loop, a significant coercivity is obtained (270 Oe). This feature is more encountered in harder ferromagnets. This confirms once again that in the case of low-dimensional magnetic systems, different properties and magnetic features are obtained, compared with their bulk counterpart. The occurrence of the coercivity in our sample is a sign of a strong planar magnetic anisotropy that makes magnetic moments harder to reverse during the applied field switching.

This strong planar anisotropy is proven also by the perpendicular-to-plane loop that shows completely different feature than the parallel loop (much slower approach to saturation). Such behavior is due to the interplay between various competing inter-cluster interactions, as well as to the enhanced surface contribution arising from the high fraction of atoms that are in surface states. The effective anisotropy constant may be estimated from the ratio between the area encompassed by the two hysteresis loops, following the Cullen & Callen [21] approach for cubic ferromagnets.

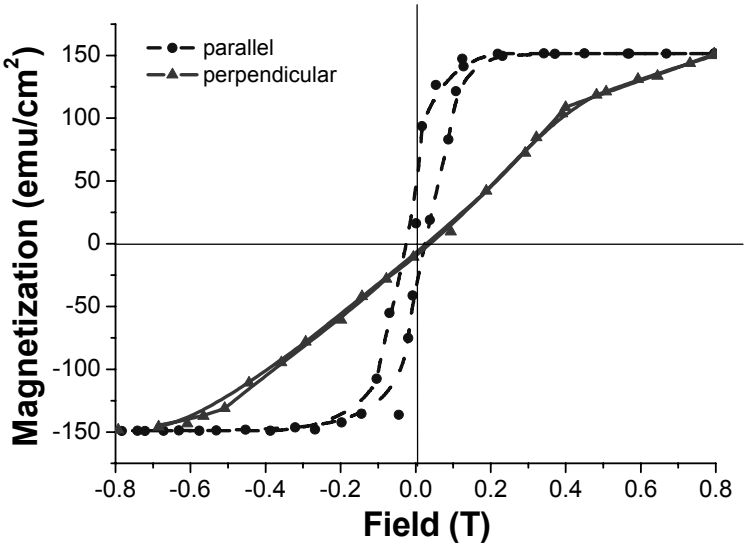

Fig. 10. Room temperature hysteresis loops with applied field parallel and perpendicular to the sample plane, for supported Fe clusters on mica.

4. Conclusions

A novel gas-stabilized cluster aggregation method was presented together with the schematics of the UHV multi-chamber facility and the principle of pick-up processes that allows creation of supersonic molecular gas beam that is subsequently used for pick-up and condensation of very fine metal clusters. Using such a method, we have been able to produce free and supported Fe clusters, core-shell Fe / Fe oxide clusters with controlled sizes. Moreover, their morpho-structural properties are thoroughly investigated.

We have proven that the cluster size is readily controlled by the metal vapor pressure inside the pick-up chamber. In its turn, this parameter is controlled by the evaporator temperature of the picked-up species (in our case the metallic Fe). By using detailed transmission electron microscopy, we showed that when the metal vapor pressure ranges between 10^{-5} and 10^{-4} mbar, the obtained Fe clusters have average cluster sizes between 2.7 and 5 nm. Electron diffraction patterns showed that the crystal symmetry is of a body-centred-cubic type and atomic force microscopy scans allow to determine that the growth mode of the Fe clusters onto the Cu grids is columnar with revealed aggregates of 10 nm size.

Using a simple method of oxidation by allowing the Fe containing molecular supersonic beam to enter a region with controlled partial pressure of oxygen, we succeeded to produce core-shell nanoparticles with metal core and continuous, uniformly thick, shell of metal oxide. These Fe / Fe oxide core-shell clusters achieve by self-organization a complex superlattice (icosahedral-type) structure, by forming multiple faceted hexagonal nanoparticles.

Supported Fe clusters on mica have the crystal structure of body-centred-cubic metallic Fe, and are superparamagnetic at room temperature, as has been revealed by X-ray diffraction and Mossbauer spectroscopy. The magnetic measurements have revealed that Fe clusters on mica exhibit pronounced coercivity, due to strong planar magnetic anisotropy exerted in the substrate plane, anisotropy induced during the deposition process.

The possibility to produce core-shell clusters using the gas-stabilised cluster aggregation UHV facility opens wide perspectives into production of several types of core-shell clusters and other nano-architectures including, for example cores with multiple shells. The extreme versatility of the method allows almost any kind of material, solids or even molecules, to be evaporated and attached to a solid core. By using multiple pick-up processes, these surface shells may be furthermore surface-functionalized for example, by attaching molecules, ligands, proteins, receptors, for a large number of biomedical applications, but also for other kind of technological applications such as: catalysis or nanosensors. The facility may as well be useful in template-assisted growth of nanoparticles to produce, for example, metal-coated complex molecules, or for synthesis of other unusual core-shell structures. For example, hydrogen-filled hollow spheres with metallic shells

have obvious technological applicability and may have huge impact as an effective hydrogen storage material.

Acknowledgements. Part of the work has been performed by O.C. at the Department of Physics, University of Leicester, UK. The financial support by the Romanian Ministry of Research under the research project PNCDI II 12-129 / 2008 is gratefully acknowledged.

References

[1] ZITOUN D., RESPAUD M., FROMEN M.C., CASANOVE M.J., LECANTE P., AMIENS C., CHAUDRET B., Phys. Rev. Lett. **89**, pp. 037203-1, 2002.
[2] CRISAN O., ANGELAKERIS M., NOGUÈS M., PAPAIOANNOU E., FLEVARIS N.K., KOMNINOU PH., KEHAGIAS TH., SOBAL N., GIERSIG M., MAGN J., Magn. Mater. **272-276,** pp. e1253-e1254, 2004.
[3] For a review of magnetic nanoparticles applications in medicine, please see: Wilfried Andrä and Hannes Nowak (Eds.) "Magnetism in Medicine: A Handbook", Wiley-VCH Interscience 2006, New York, and references therein
[4] BILLAS I.M.L., CHATELAIN A., HEER de W.A., Science **265,** p. 1682, 1994.
[5] GAMBARDELLA P., RUSPONI S., VERONESE M., DHESI S.S., GRAZIOLI C., DALLMEYER A., CABRIA I., ZELLER R., DEDERICHS P.H., KERN K., CARBONE C., BRUNE H., Science **300**, p. 1130, 2003.
[6] BOEGLIN C., STANESCU S., DEVILLE J.P., OHRESSER P., BROOKES N.B., Phys. Rev. B **66**, p. 014439, 2002.
[7] BODE M., PIETZSCH O., KUBETZKA A., WIESENDANGER R., Phys. Rev. Lett. **92**, p. 67201, 2004.
[8] KNICKELBEIN M.B., Phys. Rev. Lett. **86**, p. 5255, 2001.
[9] DOMINGO N., TESTA A.M., FIORANI D., BINNS C., BAKER S., TEJADA J., MAGN J., Magn. Mater.**316**, p. 155, 2007.
[10] LABAYE Y., CRISAN O., BERGER L., GRENECHE J.M., COEY J.M.D., J. Appl. Phys. **91**, p. 8715, 2002.
[11] CRISAN O., ANGELAKERIS M., KEHAGIAS TH., SIMEONIDIS K., GIERSIG M., FLEVARIS N.K., Acta Materialia **54**, p. 5251, 2006.
[12] BINNS C., BAKER S.H., LOUCH S., SIROTTI F., CRUGUEL H., PRIETO P., THORNTON S.C., BELLIER J.D., Applied Surface Science **226**, p. 249, 2004.
[13] BINNS C., MAHER M.J., PANKHURST Q.A., KECHRAKOS D., TROHIDOU K.N., Phys. Rev. B **66**, pp. 184413, 2002.
[14] RUTZEN M., KAKAR S., RIENECKER C., PIETROWSKI VON R., MÖLLER T., Z. Phys. D. **38**, p. 89, 1996.
[15] LINDBLAD A., BERGERSEN H., RANDER T., LUNDWALL M., ÖHRWALL G., TCHAPLYGUINE M., SVENSSON S., BJÖRNEHOLM O., Phys. Chem. Chem. Phys. **8**, p. 1899, 2006.
[16] YANG S., BRERETON S., WHEELER M., ELLIS A., MATTER S., Phys. Chem. Chem. Phys. **7**, p. 4082, 2005.
[17] YANG S., BRERETON S., ELLIS A., Int. J. Mass Spectrom. **253**, p. 79, 2006.
[18] IEVLEV D., RABIN I., SCHULZE W., ERTL G., Eur. Phys. J. D **16**, p. 157, 2001.
[19] HAGENA O.F., Z. Phys. D **4**, p. 291, 1987.
[20] BUCK U., KROHNE R., J. Chem. Phys. **105**, p. 5408, 1996.
[21] CULLEN J., CALLEN E., Phys. Rev. B **30**, p. 181, 1984.

[22] CRISAN O., HAEFTEN VON K., ELLIS A.M., BINNS C., Nanotechnology **19**, p. 505602, 2008.
[23] TEO B.K., ZHANG H., Proc. Nat. Acad. Sci. **88**, p. 5067, 1991.
[24] SUN S., MURRAY C.B., WELLER D., FOLKS L., MOSER A., Science **287**, p. 1989, 2000.
[25] CRISAN O., HAEFTEN VON K., ELLIS A.M., BINNS C., J. Nanopart. Res.**10**(1), p. 193, 2008.
[26] SHABANI A.A.T., RANCOURT D.G., LALONDE A.E., Hyp. Int. **117**, p. 117, 1998.